LIFE SCIENCES

Mucosal immunity–mediated modulation of the gut microbiome by oral delivery of probiotics into Peyer's patches

Sisi Lin[1†], Subhajit Mukherjee[1†], Juanjuan Li[1], Weiliang Hou[1], Chao Pan[1], Jinyao Liu[1,2*]

Methods capable of maintaining gut microbiota homeostasis to prevent bacterial translocation and infection under external threats are critical for multiple facets of human health but have been rarely reported. Here, we describe the elicitation of mucosal immunity to modulate the gut microbiota by oral delivery of living probiotics into Peyer's patches. Probiotics are individually camouflaged within a yeast membrane, on which the embedded β-glucan can facilitate the phagocytosis of microfold cells that locate in the intestinal epithelium. The delivery of probiotics into lymphoid follicles after oral ingestion promotes robust mucosal immune responses and notably upgrades the production of secretory immunoglobulin A. The provoked immunity positively regulates the gut microflora, which, in turn, retains gut homeostasis and provides defense against environmental attacks. In two murine models of gut barrier impairment, oral administration with camouflaged probiotics effectively prevents the breakdown of intestinal barrier and evidences limited bacterial translocation and systemic inflammation.

INTRODUCTION

The human gut microbiome consists of more than 100 trillion microorganisms and thousands of bacterial species, exerting vital functions in host immunomodulation, nutrient metabolism, maintenance of structural integrity of intestinal barrier, and defense against pathogens (*1*, *2*). The advancement of gene sequencing technologies and big data analysis has provided growing evidence that gut microbiota composition is associated with host health and also influences host response to medicines (*3*, *4*). Unfortunately, numerous external factors, such as diet, antibiotics, and pathogen invasion, can alter microbial ecology and lead to compositional and functional variations of the gut microbiome (*5*, *6*). Microbial dysbiosis has been reported to be related not only to gastrointestinal disorders, such as intestinal barrier dysfunction, inflammatory bowel disease, and colorectal cancer, but also to a variety of extraintestinal diseases, including diabetes, neurological disorders, arthritis, hepatic carcinoma, and severe acute respiratory syndrome coronavirus 2 (SARS-CoV-2) infection (*7*–*12*). Therefore, approaches capable of retaining normal homeostasis of the gut microbiota under environmental insults play a central role in human health and could transform our ability to prevent and treat diseases.

The plasticity of microbiota creates a distinct opportunity to potentially reshape gut microbial architecture and the associated biological outputs by manipulating external influencing factors (*13*–*16*). The introduction of specific nutrients, natural nucleic acids, and diverse synthetic materials has been applied to moderate the dysbiosis of gut microbes (*16*–*18*), whereas the generation of actual effectiveness needs long-term supplement and is always insufficient for occasional prevention and treatment. Alternatively, the transplantation of beneficial bacteria, including oral probiotics and fecal microbiota, has been widely exploited to restore a healthy microbial population (*19*–*22*). Despite the convenience and high patient compliance, conventional oral probiotics suffer from poor bioavailability and monomodal improvement effect (*23*). Given the concept of repopulating the gut microbiome, fecal microbiota transplantation has increasingly aroused interest and rapid acceptance in the last decade (*13*, *24*). Since its successful use in treating *Clostridium difficile* infection, fecal microbiota transplantation has been recommended for the treatment of inflammations, autoimmune disorders, metabolic dysfunctions, and certain allergic diseases (*25*). However, increased patient reluctance caused by the invasive enteral route either via a nasoenteric tube or an endoscope for ingestion has largely restricted extensive clinical practices (*26*). In addition to low compliance, the indeterminate composition inevitably results in gastrointestinal irritation, latent complication, and the risk of severe or life-threatening infections (*27*). As a result, alternative intervention strategies that only require facile operating procedures and can eliminate safety issues are highly desirable for effective modulation of the gut microbiome.

The immune system is recognized as one of the most crucial forces to shape the configuration of the gut microbiota by immunity-microbiome cross-talk (*28*). Both secretion of antimicrobial peptides from epithelial cells and germline-encoded pattern recognition receptors can mediate and influence the colonization of gut microbes. In addition to the centrality of microbiome control through epithelial cells, innate lymphoid cells are important regulators of microbial ecology, which regulate bacterial composition by secreting cytokines such as interleukins, interferon-γ, and tumor necrosis factor–α (TNF-α). Similar to the function of the innate immune system, increasing evidence discloses an essential role of the adaptive immune system in controlling the gut microbiome (*29*). In particular, B cells, producing secretory immunoglobulin A (sIgA) that can target specific bacteria and their functions, are primary contributors in the maintenance of gut homeostasis (*30*, *31*). Different from direct intervention by introducing exogenous substances or beneficial bacteria, we hence speculate whether immune manipulation could be an alternative to control the homeostasis of the gut microbiota during external attacks.

[1]State Key Laboratory of Oncogenes and Related Genes, Shanghai Cancer Institute, Shanghai Key Laboratory for Nucleic Acid Chemistry and Nanomedicine, Institute of Molecular Medicine, Renji Hospital, School of Medicine, Shanghai Jiao Tong University, Shanghai 200011, China. [2]Shanghai Key Laboratory of Gynecologic Oncology, Renji Hospital, School of Medicine, Shanghai Jiao Tong University, Shanghai 200127, China.
*Corresponding author. Email: jyliu@sjtu.edu.cn
†These authors contributed equally to this work.

Here, we report positive modulation of the gut microbiota by eliciting mucosal immunity of the intestine (Fig. 1). Camouflaged living probiotics are designed for oral delivery into Peyer's patches (PPs) given that antigen sampling through microfold cells (M cells) is the principal path in the initiation of mucosal immune responses. Beneficial bacteria are individually camouflaged inside a yeast membrane (YM) by physical coextrusion through a porous membrane. Because of the presence of embedded β-glucan on YMs, after oral ingestion, coated bacteria can facilitate Dectin-1 receptor–mediated phagocytosis of M cells distributed in the intestinal epithelium. Efficacious delivery of living bacteria into lymphoid follicles boosts strong mucosal immune responses, as reflected by markedly upgraded levels of sIgA, $CD11c^+$ dendritic cells (DCs), $CD4^+$ T cells, and IgA^+ B cells in the intestine. The augmented immunity beneficially modulates the microbiota; particularly, pathogens such as *Salmonella* and *Escherichia-Shigella* have been largely inhibited, while symbiotic bacteria have been retained successfully in the intestine suffering from infection. The maintenance of microbial structure prevents gut disturbance and provides defense against external stimulations in turn. Treatment with camouflaged bacteria effectively remits the gut barrier damage and exhibits decreased intestinal permeability in two murine models of intestinal barrier impairment. The enhanced inhibition of the translocation of bacteria and the spread of toxins and inflammatory cytokines into the system further suppresses the onset of systemic inflammation. Our work discloses how the composition and function of the gut microbiome can be retained under environmental assaults and proposes a unique platform for developing advanced oral therapeutics toward bacteria-mediated prevention and treatment.

RESULTS AND DISCUSSION

Preparation and characterization of camouflaged probiotics

Because of specific binding, yeasts with abundant surface β-glucan can be efficiently internalized by M cells characterized with embedded Dectin-1 on their membranes (*32*). Inspiringly, therapeutic agents such as small interfering RNA and nanomedicines that have been delivered by yeast capsule (YC) can improve oral bioavailability (*33*). Decoration of bacteria provides a unique tool to attach functional motifs on bacterial surface (*34*–*37*). Recently, we have wrapped with an extra membrane to generate engineered bacteria with exogenous

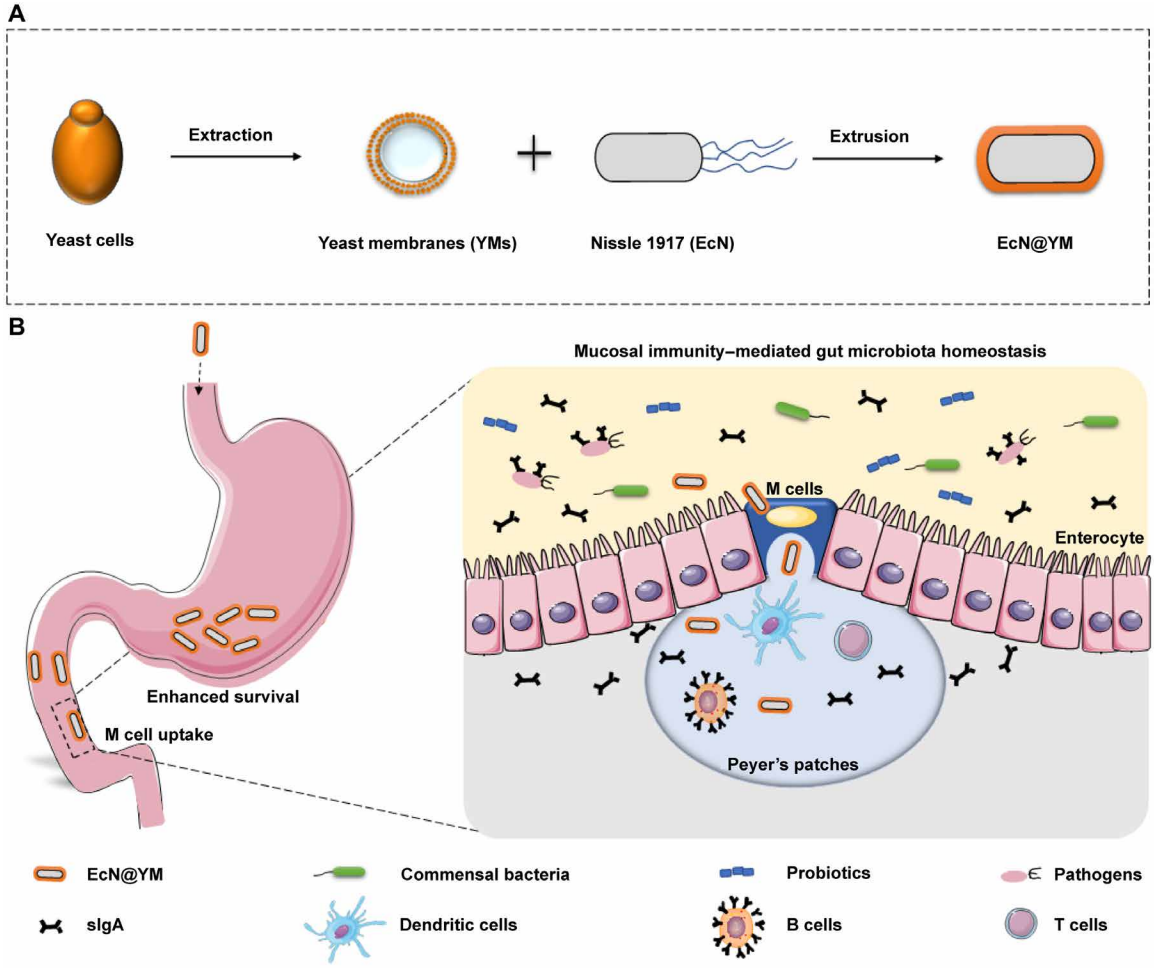

Fig. 1. Schematic illustration of mucosal immunity–mediated modulation of the gut microbiome by oral delivery of probiotics into PPs. (**A**) Preparation of EcN@YM by extruding probiotic EcN with extracted YMs through a polycarbonate porous membrane with an average pore size of 1 μm. (**B**) YMs enhance both the resistance of probiotics against gastric insults and the delivery of living bacteria into PPs through M cells, which promote robust mucosal immune responses that can positively regulate the microbiome and maintain gut homeostasis.

characteristics that can tune bacterial behaviors (*38*). For example, coating with self-assembled lipid membranes endows probiotics with enhanced resistance to extreme conditions (*35*). To take advantage of M cell–mediated antigen sampling, we wrapped *Escherichia coli* Nissle 1917 (EcN), a typical probiotic, with a YM coating to increase accumulation in PPs following oral administration. To prevent potential degradation of β-glucan (*39*), YMs were prepared by mechanically squeezing yeast cells with glass beads (fig. S1). Simply fusing EcN with YMs via physical extrusion through a porous polycarbonate membrane with an average size of 1 μm could generate YM-coated EcN (EcN@YM). Under laser scanning confocal microscopy (LSCM) imaging, EcN expressing mCherry (red) were coated with YMs (blue) stained with calcofluor-white, a dye selectively binding to yeast wall (Fig. 2A). The coating was further confirmed by transmission electron microscopy (TEM) and scanning electron microscopy (SEM) observation (Fig. 2B and fig. S2, A to C). In contrast to uncoated cells, EcN@YM were surrounded with an additional thick membrane. Zeta potential of EcN was increased from −25.0 ± 5.72 to −13.1 ± 1.77 mV after coating with a less negatively charged YM membrane (Fig. 2C). Dynamic light scattering (DLS) measurement suggested that the average size of EcN@YM was 1186.3 nm (fig. S2, D and E), which was suitable for the uptake by M cells (*40*). Flow cytometric analysis showed that the mean fluorescence intensity of EcN@YM was ~10 times higher than uncoated EcN, validating an encapsulation efficiency of 85.8% (Fig. 2, D and E). These results indicated that EcN were successfully yet highly efficiently coated with YMs via a simple mechanical extrusion. Cell counting kit-8 (CCK-8) assay showed limited fluctuations on the viability of bacteria after coating, demonstrating that both the preparation procedure and the coating itself had a negligible impact on EcN vitality (Fig. 2F). Meanwhile, EcN@YM exhibited limited toxicity against Caco-2 cells even with bacterial number increasing up to 1×10^8 colony-forming units (CFUs) (fig. S3). In consideration of the importance of β-glucan on M cell uptake, the stability of the associated β-glucan on YMs was monitored by culturing under simulated gastrointestinal conditions for the indicated time points. As shown in Fig. 2G, the level of β-glucan remained consistent in both simulated gastric fluid (SGF) and simulated intestinal fluid (SIF) even with incubation time extending up to 4 hours, suggesting an extraordinary stability of the membrane β-glucan.

Stability and viability of EcN@YM in the gastrointestinal tract

Before reaching M cells, the delivered probiotics would suffer from gastrointestinal environments after oral ingestion, such as gastric acid and bile salts, which could cause instability and even more bacterial deactivation (*34*, *35*, *38*). We next measured the β-glucan level of EcN@YM in both SGF and SIF to assess whether the unfriendly conditions could degrade β-glucan presented on the surface of the bacteria. The β-glucan was stable and remained unaffected with cultivation time increasing up to 4 hours (Fig. 3A). Similar results were observed for EcN@YM that were incubated in SIF, verifying the notable stability of β-glucan on coated bacteria. In addition, we measured the stability of the coating and the protective role of YMs in the viability of EcN. After incubation of EcN@YM in SIF for the indicated time points, LSCM and TEM images displayed that uncoated EcN emerged after 1-hour incubation and the removal of the coating increased with culture time increasing from 2 to 6 hours (fig. S4). As expected, coating with a YM could lift the survival of EcN in gastric acid, which was in stark contrast with complete deactivation of uncoated bacteria (Fig. 3B and fig. S5). Comparable protection effects were observed for coated EcN that were incubated with cholic acid and SIF, respectively (Fig. 3, C and D, and figs. S6 and S7). In vivo tolerance of coated bacteria was further evaluated in the gastrointestinal tract of mice. The radiant efficiencies of the mice and the sectioned gastrointestinal tracts were calculated by in vivo imaging system (IVIS) and showed relatively higher values of mice dosed with EcN@YM at each indicated time point, in contrast to mice administrated with EcN (fig. S8). To quantify the number of survived EcN, intraluminal contents were separately collected from the stomach, small intestine, cecum, and colon for bacterial plate counting. The results plotted in Fig. 3 (E to H) indicated that the average amount of living EcN in each location from mice orally delivered with EcN@YM was higher than EcN at 1, 2, 3, and 4 hours after administration, respectively. The total survivals at 1, 2, 3, and 4 hours after dosing were significantly enhanced after coating with YMs, demonstrating the protective effects of the coating on bacterial viability under the gastrointestinal environments (Fig. 3, I to L). These results suggested that the membrane β-glucan was stable, and the viability of coated EcN could be improved after oral ingestion, which would benefit the delivery of probiotics into PPs.

Uptake of camouflaged probiotics by M cells

To validate YM coating–mediated delivery into PPs, the uptake efficiency of EcN by M cells was assessed both in vitro and in vivo. In a Transwell cell culture experiment, equal amounts of EcN and EcN@YM were added to the apical chamber of the inserts after the differentiation of M cells from Caco-2 cells was ensured by detecting alkaline phosphatase (AP) activity (fig. S9) (*41*). The numbers of EcN@YM translocated into a basolateral medium were counted following coculture for 3 and 6 hours, respectively. As depicted in Fig. 4A, the counts of EcN@YM were found to be more than five times higher than EcN after 3 hours of incubation under the same condition. With culture time extending to 6 hours, the number of translocated bacteria further increased to ~11-fold higher than uncoated EcN (Fig. 4B). Having confirmed the significantly enhanced translocation in vitro, we further examined the cellular uptake of EcN@YM by M cells in mice by direct injection into the intestinal lumen according to the method described previously (*42*). Both phosphate-buffered saline (PBS) and equivalent uncoated EcN were applied as controls. At 1.5 hours after injection, the PPs were collected and homogenized for culture on lysogeny broth (LB) agar plates for bacterial quantification. Expectedly, EcN were not observed for PPs sampled from mice injected with PBS (Fig. 4C and fig. S10). Coating with YMs significantly elevated the count of bacteria transported into the PPs, which was nearly two times higher than uncoated EcN. The promoted accumulation of EcN@YM was further visualized by LSCM imaging of the fixed tissues of the PPs. As displayed in Fig. 4D, an apparent higher density of the red dots, indicating EcN expressing mCherry, was observed for PPs harvested from mice dosed with EcN@YM.

The enrichment of EcN in PPs following oral administration was assessed to further verify that YM coating could facilitate the phagocytosis of M cells. Mice were dosed with 1×10^8 CFUs of EcN@YM daily by oral gavage and euthanized at the indicated time points. Plate counting of the homogenized PPs showed that EcN appeared in some of the mice treated with coated bacteria at 4 hours after the first dose, which was not observed for mice that received uncoated EcN (Fig. 4E). Notably, with the dosing period prolonged to 7 days, all mice

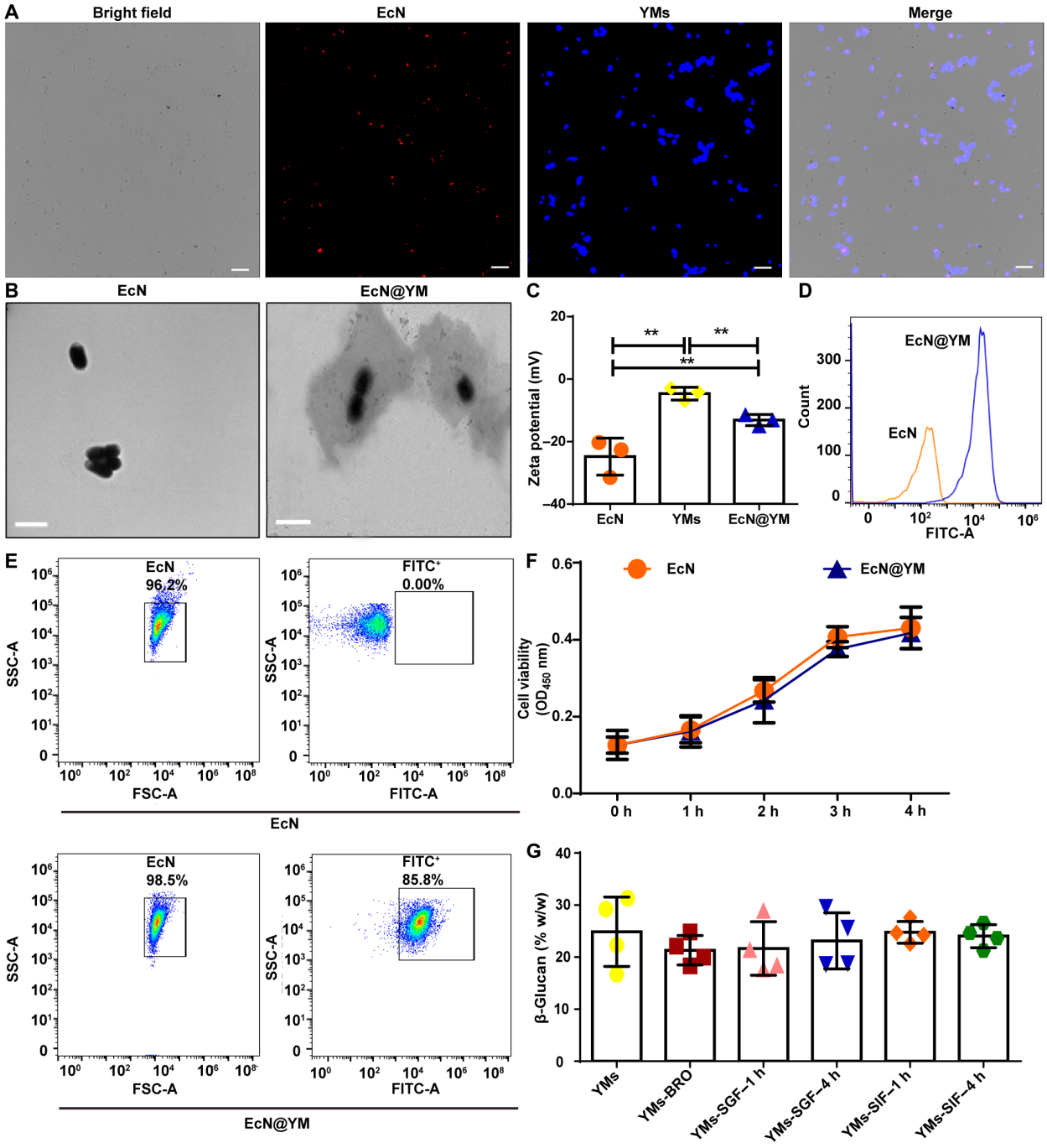

Fig. 2. Preparation and characterization of EcN@YM. (**A**) LSCM images of EcN@YM. The red channel shows EcN expressing mCherry, and the blue channel indicates YMs stained with calcofluor-white. Scale bars, 20 μm. (**B**) Typical TEM images of EcN and EcN@YM. Scale bars, 2 μm. (**C**) Zeta potentials of EcN, YMs, and EcN@YM, respectively. $^{**}P < 0.01$. (**D** and **E**) Flow cytometric analysis of EcN and EcN@YM. YMs were labeled with fluorescein isothiocyanate (FITC). Error bars represent SD ($n = 3$). (**F**) Bacterial viabilities of EcN and EcN@YM, respectively. The viability was evaluated by measuring optical density at 450 nm (OD_{450}) at 1-hour interval using CCK-8 assay. (**G**) Level of β-glucan on YMs under different treatments including glass bead broken only (YMs-BRO), glass bead broken and incubation with SGF for 1 hour (YMs-SGF–1 h) or 4 hours (YMs-SGF–4 h), and glass bead broken and treatment with SIF for 1 hour (YMs-SIF–1 h) or 4 hours (YMs-SIF–4 h). FSC-A, forward scatter area; SSC-A, side scatter area.

in the EcN@YM group presented numerous EcN in the PPs, whereas it was rare that bacteria emerged in mice administrated with uncoated EcN (Fig. 4F). The significantly enhanced accumulation of EcN achieved by camouflage was maintained up to 3 weeks, suggesting the YM-mediated transport into PPs following oral delivery (Fig. 4G).

Stimulation of intestinal mucosal immunity by EcN@YM

As visualized by ex vivo imaging, EcN appeared on mesenteric lymph nodes (MLNs) only 4 hours after oral gavage, which should be rapidly translocated from the PPs (Fig. 5A). In good agreement with the enrichment of EcN in the PPs, dosing with coated EcN

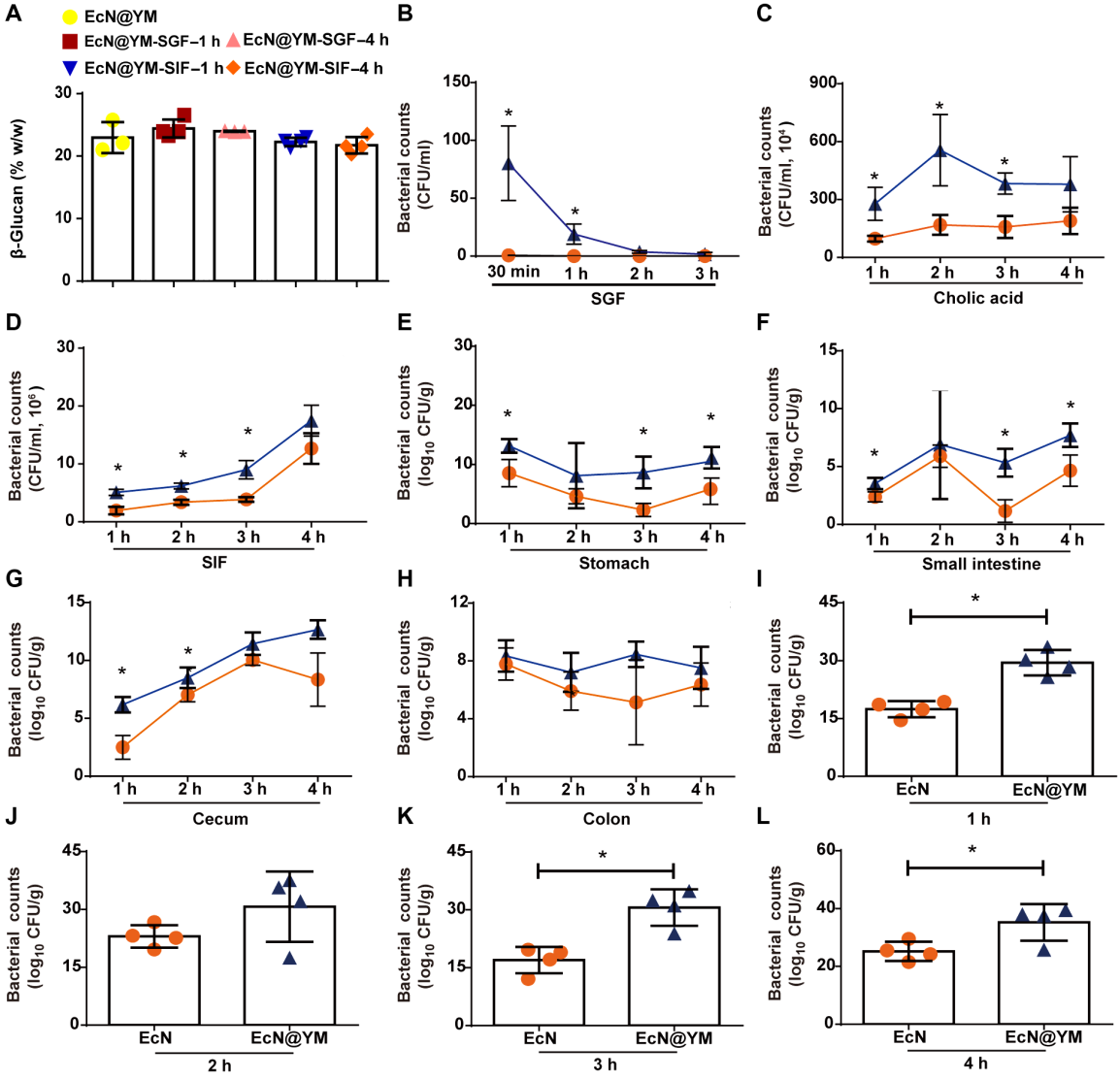

Fig. 3. Stability of EcN@YM in gastrointestinal environments. (**A**) Level of β-glucan on EcN@YM under different treatments including incubation with SGF for 1 hour (EcN@YM-SGF–1 h) or 4 hours (EcN@YM-SGF–4 h) and SIF for 1 hour (EcN@YM-SIF–1 h) or 4 hours (EcN@YM-SIF–4 h), respectively. (**B** to **D**) Survivals of EcN (orange circle) and EcN@YM (blue triangle) after treatment with (B) SGF, (C) cholic acid, or (D) SIF ($n = 3$). (**E** to **H**) Counts of bacteria in the (E) stomach, (F) small intestine, (G) cecum, and (H) colon at the indicated time points after gavage of 1×10^8 CFUs of EcN or EcN@YM ($n = 4$). (**I** to **L**) Total amounts of bacteria in the gastrointestinal tract at (I) 1, (J) 2, (K) 3, and (L) 4 hours after gavage. Error bars represent SD, $^*P < 0.05$.

expressing mCherry displayed higher radiant efficiency in comparison with uncoated bacteria, suggesting the aggregation of more EcN in the lymph nodes (Fig. 5B). Quantification analysis further illustrated that EcN@YM accumulated nearly eightfold higher than EcN (Fig. 5C). Encouraged by the rapid yet efficient delivery of EcN through M cells, we next investigated whether robust mucosal immune responses could be initiated. sIgA, one of the most important effectors on intestinal mucosal immunity, plays multiple roles in the maintenance of gut homeostasis, including pathogen resistance, anti-inflammation, mucus secretion, and adjustment of tight junction expression (*30*, *31*). The induction of a sIgA response by microbial antigens is a fundamental step toward the establishment and maintenance of microbial homeostasis (*43*). Studies have highlighted that antigens recognized and sampled through M cells are main contributors to the efficient initiation of a homeostatic sIgA response (*44*, *45*). Although some probiotics are able to motivate sIgA production, the promotion has been limited in infants as the regular sIgA response after ablactation is dependent on the sampling of microbial antigens by M cells (*46*, *47*). We therefore measured the level of sIgA that was released into the intestinal fluid (Fig. 5G). In contrast to PBS control, mice dosed with EcN presented a reduced level of sIgA, which could be explained by the neutralization with numerous microbial antigens present on uncoated bacteria in the small intestine (*48*). It was noted that in comparison with EcN treatment, YMs alone could upgrade the production of sIgA due to their immune activity (*49*), while the promotion was limited to a short period of 4 hours following ingestion. Excitingly, the reinforced transport of EcN@YM by M cells could induce remarkable immune responses

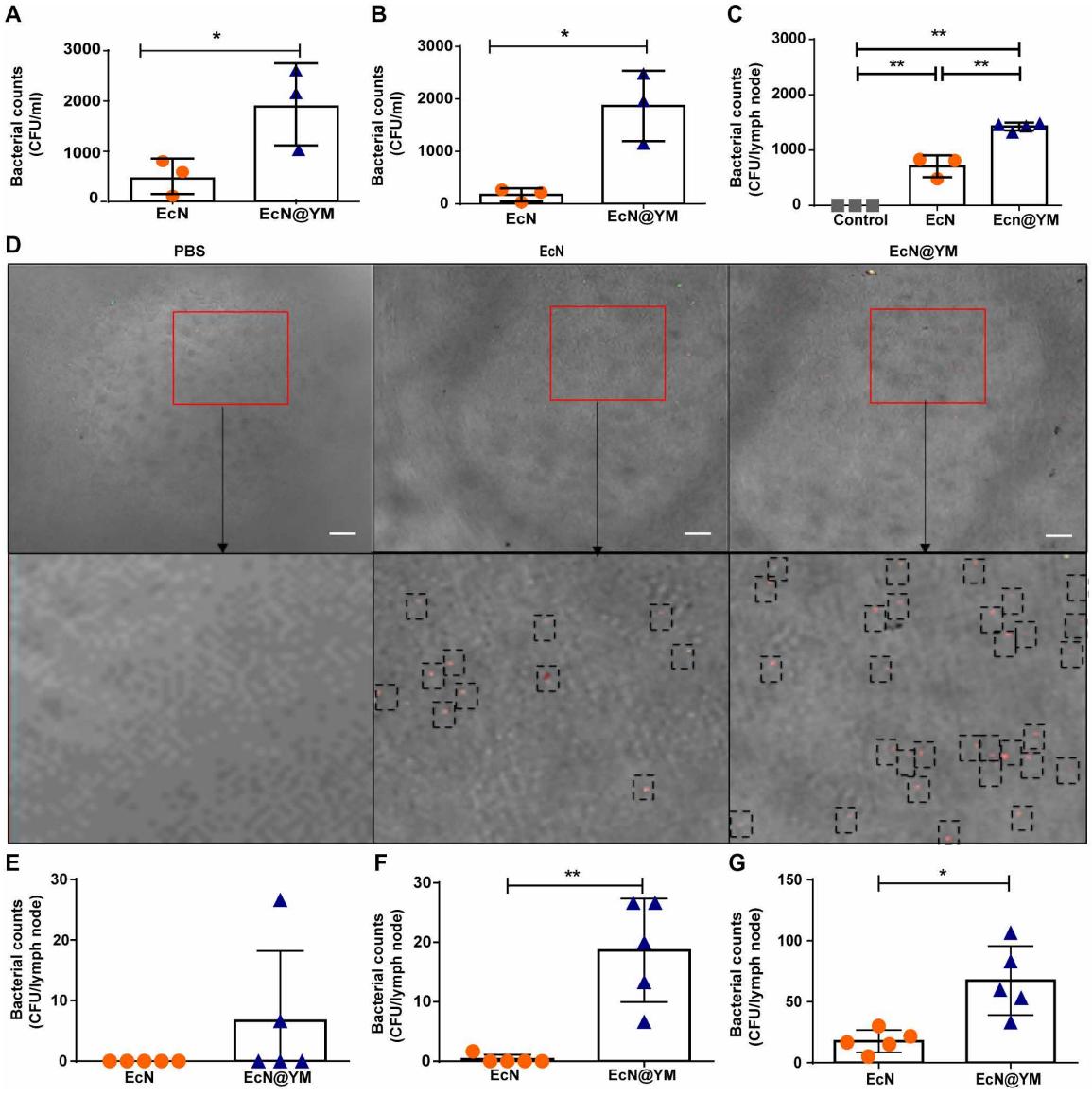

Fig. 4. Uptake of EcN@YM by M cells. (**A** and **B**) Amount of EcN in the basolateral chamber translocated from the apical side of Transwell inserts after coculture with M cells for (A) 3 and (B) 6 hours, respectively. (**C**) Counts of EcN in PPs at 1.5 hours after lumen injection of PBS, EcN, and EcN@YM, respectively. Mice were anesthetized, and the gut loop containing PPs was injected with 50 μl of PBS and 1×10^8 CFUs of EcN or EcN@YM. (**D**) Representative LSCM images of EcN expressing mCherry (red) in PPs collected at 1.5 hours after lumen injection. (**E** to **G**) Counts of EcN in PPs at (E) 4 hours, (F) 7 days, and (G) 3 weeks after treatment. Mice were daily gavaged with 5×10^7 CFUs of EcN or EcN@YM. Error bars represent SD ($n = 3$ to 5); $^*P < 0.05$ and $^{**}P < 0.01$.

at 4 hours after administration, as certified by the significantly increased sIgA concentration in the intestine compared with the other groups. This increment could be ascribed to both the production of a higher level of sIgA resulting from the promoted uptake by M cells and the decreased binding of sIgA with EcN as the antigens were shielded by YM coating. Furthermore, the sIgA level and the aggregation of EcN in MLNs after ingestion with EcN@YM remained the highest in all the treated mice even with the treatment period prolonged to 7 days (Fig. 5, D to G). We further measured the immune cells that were actively involved in the regulation of sIgA secretion (*43*). The levels of $CD11c^+$ DCs, $CD3^+$ T cells, $CD4^+$ T cells, $CD8^+$ T cells, and IgA^+ B cells both in PPs and MLNs increased following daily administration of a dose of 5×10^7 CFUs of EcN@YM for 7 days (Fig. 5, J to Q, and fig. S11). The stimulation of these immune cells was accompanied with increased expression of activation markers CD80 and CD86 on $CD11c^+$ DCs (figs. S12 and S13). The elicited immune responses could be ascribed to sufficient accumulation of EcN@YM in PPs and the immunoadjuvant activity of YMs (*49*). In addition, it was worth noting that the key inflammatory cytokines including interleukin-6 (IL-6) and TNF-α could return to the normal level, although there was a temporary increase following the first dose (Fig. 5, H and I). Namely, the appearance of a similar inflammatory response to conventional EcN indicated the limited side effect of EcN@YM used as oral probiotics.

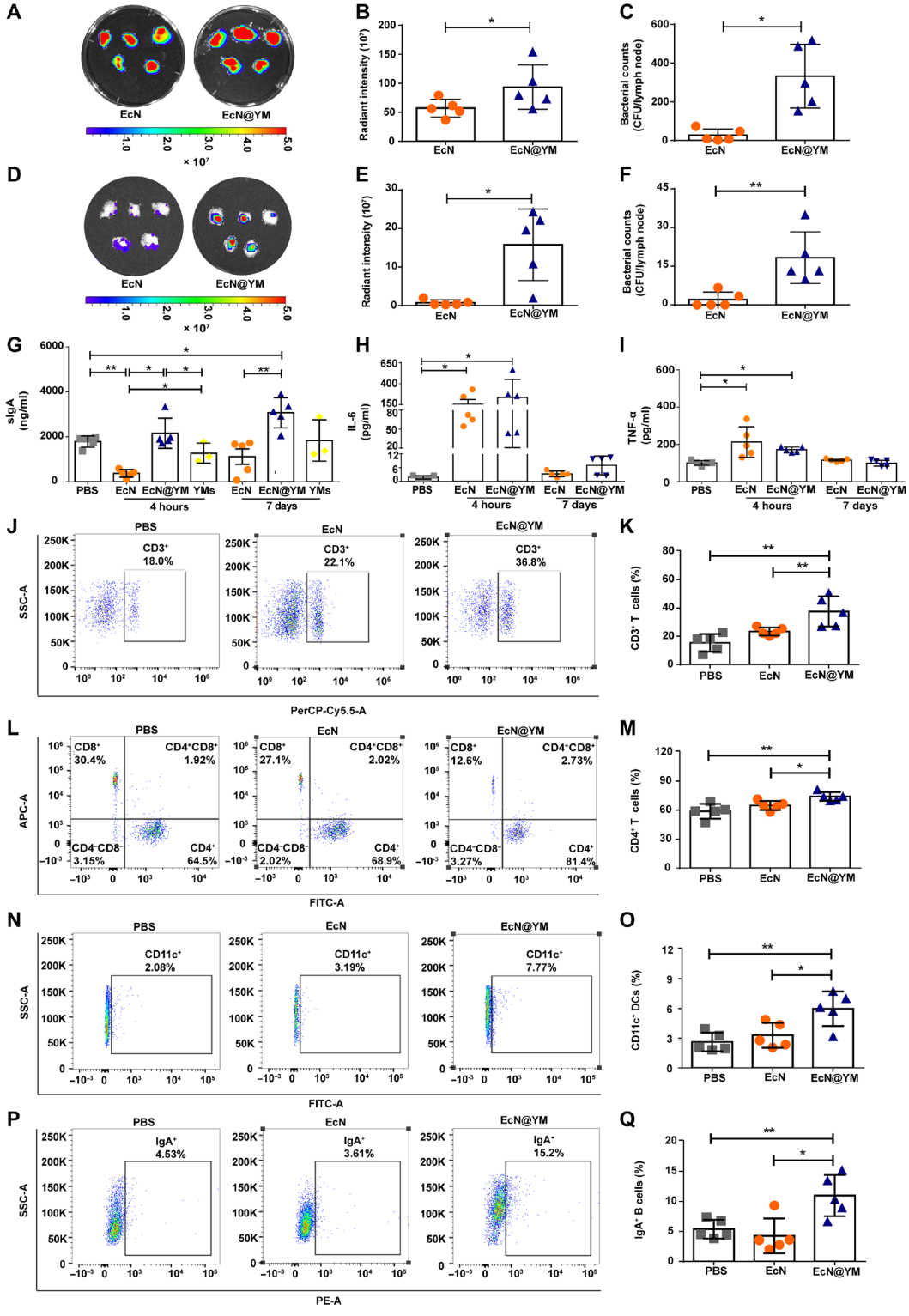

Fig. 5. Mucosal immune responses elicited by EcN@YM. (**A** to **F**) Representative IVIS images, radiant fluorescence intensity, and bacterial counts of MLNs at (A to C) 4 hours and (D to F) 7 days after gavage of 5×10^7 CFUs of EcN or EcN@YM. (**G**) Level of sIgA in the intestinal fluid after treatment with PBS, EcN, EcN@YM, and YMs, respectively. (**H** and **I**) Expression levels of (H) IL-6 and (I) TNF-α in plasma after treatment with PBS, EcN, and EcN@YM, respectively. (**J** to **Q**) Flow cytometric analysis and the percentages of (J and K) $CD3^+$ T cells, (L and M) $CD4^+$ T cells, (N and O) $CD11c^+$ DCs, and (P and Q) IgA^+ B cells in lymphocytes sampled from PPs after daily gavage of 0.2 ml of PBS and 5×10^7 CFUs of EcN or EcN@YM for 7 days. T cells, DCs, and B cells were labeled with antibodies of anti–CD3-PerCP-Cy5.5/anti–CD4-FITC/anti–CD8–allophycocyanin (APC), anti–CD11c-FITC/anti–CD86-APC/anti–CD80–phycoerythrin (PE), and anti–CD45R/B220-PE-Cy7/anti–CD138-APC/anti–IgA-PE, respectively. Error bars represent SD ($n = 3$ to 5); $^*P < 0.05$ and $^{**}P < 0.01$.

Maintenance of gut microbial homeostasis under external stimuli

To understand the ability to maintain gut microbial homeostasis under environmental insults, we studied the variation of the composition of the gut microbiota in mice suffering from pathogen invasion and intestinal manipulation (IM), respectively. Mice were daily dosed with oral EcN@YM for 7 days and then infected with 5×10^7 CFUs of *Salmonella* by gavage. Three days after infection, all mice were euthanized, and the microbial structure was analyzed by 16*S* ribosomal RNA gene sequencing. Healthy mice and infected mice separately pretreated with PBS and EcN were used as controls. As validated in Fig. 6, pretreatment with uncoated EcN exhibited a negligible effect on the maintenance of the gut microbiome as the microbial composition approximated infected mice that were pretreated with PBS (Fig. 6, A and B, and fig. S14). Notably, the microbial structure of mice pretreated with EcN@YM was closer to that of healthy mice. In particular, there was a decrease in Proteobacteria, which included a wide variety of pathogens (*50*), such as *Salmonella* and *Escherichia-Shigella* (Fig. 6C). Meanwhile, an increase in Bacteroidetes that consisted of most of the symbiotic bacteria (*51*) was achieved, indicating that pretreatment with EcN@YM could resist the disturbance of microbial homeostasis by pathogen infection (Fig. 6, D and E). The maintenance of a healthy microbial structure against external invasion was mainly attributed to the enhanced production of sIgA, which served as an important regulator in the control of a homeostatic gut microbiota (*45*). We further analyzed the alteration of the microbiome in mice that experienced IM (*52*). Physical injury of the intestine resulted in a clear decrease in microbiota diversity (Fig. 6F). Similarly, pretreating with uncoated bacteria revealed a limited beneficial effect on maintaining microbiota homeostasis, as supported by accordant diversity to that of manipulated mice pretreated with PBS (Fig. 6, G and H, and fig. S15). On the contrary, the application of EcN@YM led to a healthy microbial ecosystem that was almost identical to that of healthy mice, even though they underwent IM. In brief, these data verified the capability of the microbiome regulated by provoked mucosal immunity to withstand unfriendly surroundings.

Prevention of intestinal barrier impairment

The disruption of intestinal microbial homeostasis is well acclaimed to be the driving force of the pathogenesis and progression of numerous intractable diseases (*53*). In particular, intestinal barrier injury, one of many intestinal disorders, tendentiously leads to cytokine storm and refractory chronic inflammation due to constant systemic infiltration of a vast array of lumen antigens, inflammatory cytokines, and toxins (*54*). However, specific prevention and treatment for gut barrier dysfunction are still unavailable in the clinical setting (*55*). Encouraged by immunity-mediated modulation of the gut microbiota that could resist external stimuli, we hence explored the potential of EcN@YM to prevent the occurrence of gut barrier injury. To this end, two murine models of barrier impairment were developed to substantiate preventive efficacy (*56*). Mice were pretreated with PBS, EcN, or EcN@YM for 7 days before inducing intestinal barrier injury. Healthy mice were used as a control.

As illustrated in Fig. 7A, the pretreated mice were orally administrated with streptomycin and then with 5×10^7 CFUs of *Salmonella*. All mice were euthanized for sampling 3 days after infection. The infection caused obvious damage to the intestinal barrier of mice pretreated with PBS, as reflected by severe submucosal edema, depletion of goblet cells, and an increase in intestinal permeability (Fig. 7, B to E). The increased levels of lipopolysaccharide (LPS) and inflammatory cytokines including IL-6 and TNF-α in plasma further indicated that the impairment of the intestinal barrier resulted in systemic inflammation (Fig. 7, F to H). Clearly, among all the treatment groups, the breakdown of the intestinal barrier was prevented most effectively by pretreating with EcN@YM. Clearly, only treatment with EcN@YM could significantly reduce the invasion of *Salmonella* (Fig. 7, D to L). Furthermore, EcN@YM treatment could decrease the levels of IL-6 and TNF-α and the pathological score even compared with EcN (Fig. 7, D, G, and H). In addition, prevention with EcN@YM could significantly decrease the translocation of *Salmonella* to both proximal and remote organs (Fig. 7, I to L). In comparison to uncoated bacteria, EcN@YM showed less *Salmonella* translocated to proximal tissues including PPs and MLNs, although both uncoated and coated EcN diminished the extent of translocation to distant organs, such as the spleen and liver. The enhanced prevention by EcN@YM could be explained by more efficient induction of the release of sIgA in the intestine. The second mouse model was induced by IM (Fig. 8A), which led to not only abnormal intestinal motility but also intestinal barrier impairment (*52*). Similarly, IM caused an increase in the infiltration of inflammatory cells in the muscular layer and the depletion of goblet cells, which were accompanied by the increased intestinal permeability (Fig. 8, B to D). It was noticed that pretreatment with EcN could not resist the stimulation from physical manipulation, while preventive intervention with EcN@YM significantly reduced the intestinal permeability and the level of LPS (Fig. 8, D and E). EcN@YM treatment could also significantly decrease the production of IL-6 and TNF-α compared to EcN (Fig. 8, F and G). We further detected bacterial translocation to assess the degree of intestinal barrier impairment. As shown in Fig. 8 (H to O), the translocation of both aerobic and anaerobic bacteria was greatly increased after IM. Other than EcN, pretreatment with EcN@YM could decrease the transfer of aerobic bacteria in PPs, MLNs, spleen, and liver (Fig. 8, H to K). Prevention with EcN@YM demonstrated enhanced resistance to the translocation of anaerobic bacteria in comparison to that of uncoated EcN (Fig. 8, L to O). These results indicated that mucosal immunity–mediated homeostasis of the gut microbiota could effectively lower the occurrence of intestinal barrier impairment under environmental stimuli.

In summary, we report the initiation of mucosal immunity to regulate the gut microbiome by orally delivering living probiotics into PPs. Inspired by the specific binding between β-glucan anchored on yeast surface and Dectin-1 embedded on the membrane of M cells, we design and prepare M cell preferred oral probiotics by wrapping with a YM coating. To examine whether the camouflaged probiotics could be delivered into PPs through M cells with the help of the coating, we first confirm that YMs can protect coated EcN from the insults of the gastrointestinal environments. Furthermore, to ensure the delivery of living bacteria into PPs, the remarkable stability of β-glucan that is important for M cell uptake is confirmed under a condition simulating the intraluminal microenvironment of the gastrointestinal tract. To measure the efficiency of M cell uptake, coculture of M cells with EcN with or without a YM coating is performed in vitro, and coated bacteria show a significant increase in internalization. The enhanced uptake is further supported by a promoted accumulation of EcN in PPs and MLNs sampled from mice received with coated bacteria. As expected, the sIgA level in the intestinal fluid is increased greatly following oral ingestion of the coated probiotics. The elicited mucosal immunity positively shapes

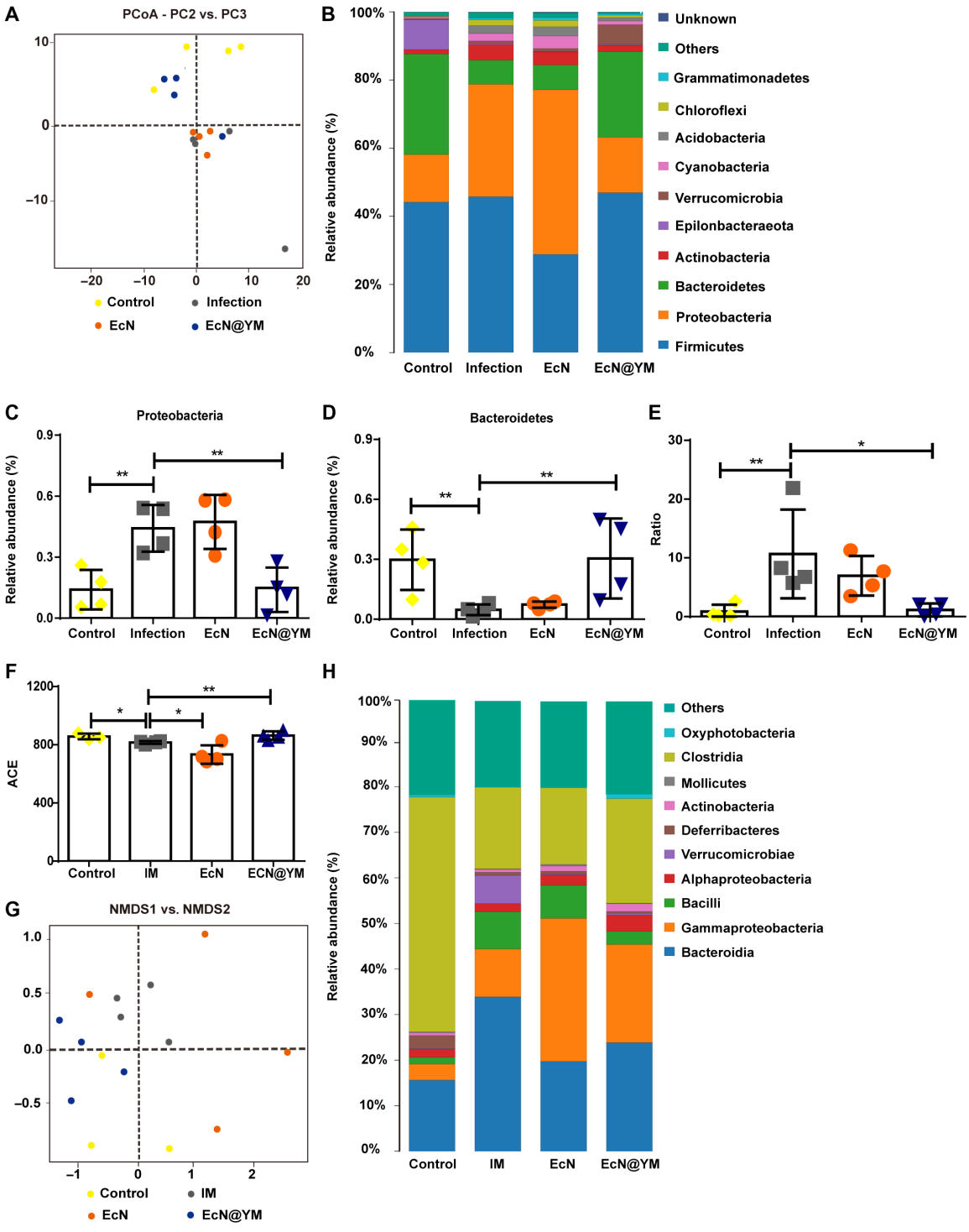

Fig. 6. Maintenance of the gut microbiome under external stimuli. (**A** and **B**) Results of (A) principal coordinates analysis (PCoA) and (B) taxonomic analysis at the phylum level of the gut microbiota from the infected mice. Alpha diversity, which reflects the species richness of individual samples and the species diversity, was presented with ACE; beta diversity, which is used to compare the species diversity in community composition and structure between different groups, was analyzed with PCoA or non-metric multidimensional scaling (NMDS). Mice were daily pretreated with PBS and 5×10^7 CFUs of EcN or EcN@YM for 7 days and subsequently infected with 5×10^7 CFUs of *Salmonella*. (**C** and **D**) Relative abundances of (C) Proteobacteria and (D) Bacteroidetes in the gut microflora. (**E**) Ratio of the relative abundance of Proteobacteria to Bacteroidetes. (**F** to **H**) Values of (F) ACE index, (G) NMDS, and (H) bacterial taxonomic analysis at the class level in mice after IM operation. Mice were daily pretreated with PBS and 5×10^7 CFUs of EcN or EcN@YM for 7 days before the operation. Error bars represent SD ($n = 4$); *$P < 0.05$ and **$P < 0.01$.

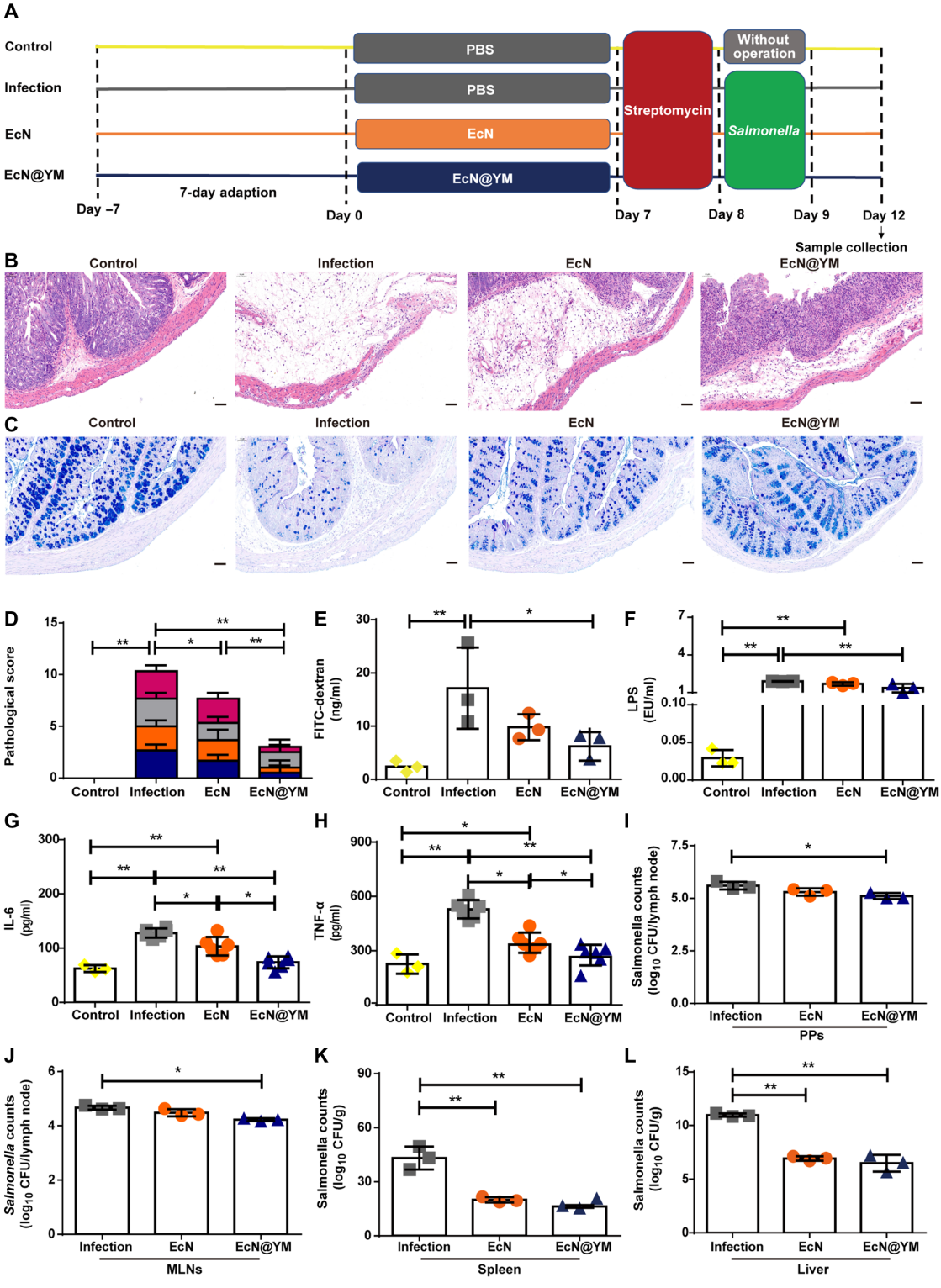

Fig. 7. Effect of EcN@YM on the prevention of intestinal barrier impairment in *Salmonella* infection. (**A**) Design of the animal study. After adaption raise for 7 days, mice were daily gavaged with 0.2 ml of PBS and 5×10^7 CFUs of EcN or EcN@YM for 7 days and then administrated with 20 mg of streptomycin. Mice were orally dosed with 5×10^7 CFUs of *Salmonella*, and samples were collected 3 days after infection. (**B**) Representative hematoxylin and eosin staining images of the cecum tissue. Scale bars, 50 μm. (**C**) Typical Alcian Blue (AB)/Periodic Acid-Schiff (PAS) staining images of goblet cells in the colon tissue. Scale bars, 50 μm. (**D**) Pathological scores based on the sums of epithelial integrity (pink), submucosa edema (gray), infiltration of inflammatory cells (orange), and goblet cell depletion (blue). (**E**) Intestinal permeability assessed by measuring FITC-dextran in plasma. (**F** to **H**) Levels of (F) LPS, (G) IL-6, and (H) TNF-α in plasma. (**I** to **L**) Counts of *Salmonella* in (I) PPs, (J) MLNs, (K) spleen, and (L) liver, respectively. Tissue samples were homogenized, spread onto LB agar plates, and incubated overnight at 37°C for bacterial counting. Error bars represent SD ($n = 3$ to 6); $^*P < 0.05$ and $^{**}P < 0.01$.

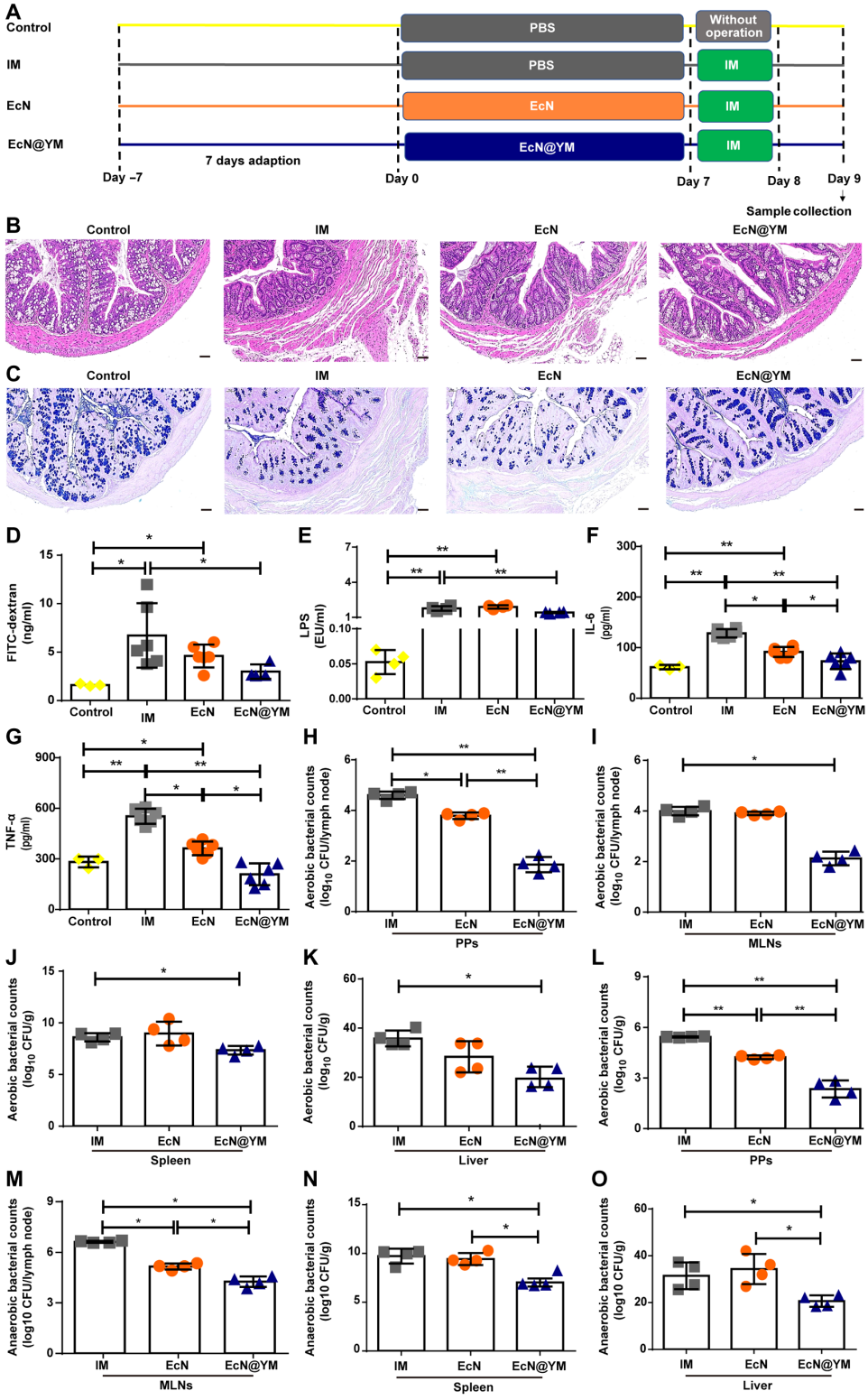

Fig. 8. Effect of EcN@YM on the prevention of intestinal barrier impairment under IM. (**A**) Design of the animal study. After adaption raise for 7 days, mice were daily dosed with 0.2 ml of PBS and 5×10^7 CFUs of EcN or EcN@YM for 7 days and then subjected to IM operation. Samples were collected 24 hours after operation. (**B**) H&E staining images of the colon tissue. Scale bars, 50 μm. (**C**) AB/PAS staining images of goblet cells in the colon tissue. Scale bars, 50 μm. (**D**) Intestinal permeability assessed by measuring the level of FITC-dextran in plasma. (**E** to **G**) Levels of (E) LPS, (F) IL-6, and (G) TNF-α in plasma. (**H** to **K**) Counts of aerobic bacteria in (H) PPs, (I) MLNs, (J) spleen, and (K) liver, respectively. (**L** to **O**) Amounts of anaerobic bacteria in (L) PPs, (M) MLNs, (N) spleen, and (O) liver, respectively. Sampled tissues were homogenized, spread onto blood agar plates, and cultured overnight at 37°C under anaerobic conditions for bacterial counting. Error bars represent SD ($n = 3$ to 6); *$P < 0.05$ and **$P < 0.01$.

the microbiota, which maintains homeostasis under external stimulations. In turn, the maintenance of microbiome composition protects the intestinal barrier from injury under pathogen infection and IM, as demonstrated by decreased intestinal permeability, enhanced inhibition of the translocation of bacteria and toxins, and suppressed systemic inflammation. This work opens a window for maintaining the composition and function of the gut microbiome under external stimuli and suggests an alternative to develop innovative therapeutics for bacteria-mediated therapies.

MATERIALS AND METHODS

Materials and strains

EcN and *Salmonella typhimurium* were purchased from China General Microbiological Culture Collection Center. Caco-2 and Raji cell lines were obtained from the American Type Culture Collection. Baker's yeast was obtained from Lesaffre. Minimum Eagle's medium (MEM), RPMI 1640, fetal bovine serum, and antibiotic/antimycotic solution were purchased from Thermo Fisher Scientific. Calcofluor-white stain was purchased from Sigma-Aldrich. The β-Glucan assay kit was purchased from Megazyme. Fluorescence-activated cell sorting antibodies including anti-mouse CD3-PerCP Cy5.5, CD4–fluorescein isothiocyanate (FITC), CD8–allophycocyanin (APC), CD11c-FITC, CD80–phycoerythrin (PE), CD86-APC, CD45R/B220-PE-Cy7, and CD138-APC were purchased from eBioscience. IgA-PE was purchased from Thermo Fisher Scientific. Plasmids pBBR1MCS2-Tac-mCherry (kanamycin resistance) and all other reagents were purchased from domestic suppliers and used as received.

Preparation of YMs

Baker's yeast (20 g) was suspended in 300 ml of 1 M sodium hydroxide. The suspension was heated to 80°C for 1.5 hours and centrifuged at 3000 rpm for 10 min. The pellet was rinsed twice with deionized water, dispersed in hydrochloric acid at pH 4, and incubated at 60°C for 1.5 hours. The sample was collected by centrifugation at 3000 rpm for 10 min and thoroughly washed with deionized water twice. Subsequently, the pellet was rinsed with isopropyl alcohol four times and with acetone two times. The YC was collected by centrifugation and dried under vacuum at room temperature. To prepare YMs, YC (10 mg/ml) was broken by vortexing with glass beads (300 to 500 nm) for 2 hours at room temperature.

Fabrication of EcN@YM

EcN with pBBR1MCS2-Tac-mCherry plasmid were grown in LB agar plates containing kanamycin antibiotic at 37°C for 4 hours with shaking at 200 rpm. Bacteria were collected by centrifugation at 7000 rpm for 10 min and resuspended in cold PBS. YMs (300 μl) and EcN (700 μl) were mixed and cultured at room temperature for 1 hour with shaking at 500 rpm. Then, the mixture was extruded 21 times through a polycarbonate porous membrane with a pore size of 1 μm by using a mini extruder (Avanti Polar Lipids, USA).

Characterization of EcN and EcN@YM

The morphology of bacteria was measured by TEM and SEM. A drop of 10 μl of EcN or EcN@YM was loaded onto a Formvar/carbon 300-mesh grid for 30 min and rinsed twice with distilled water. After air drying the samples were observed by TEM (Tecnai G2, Thermo Fisher Scientific, USA). For SEM (Sirion 200, USA) measurement, samples were dropped on a silicon wafer separately after serial dehydration in 30, 50, 70, 80, 90, and 100% ethanol for 10 min. The size and zeta potential of EcN and EcN@YM were measured by DLS (Zetasizer Nano ZS, Malvern, UK). EcN coated with FITC-labeled YM was measured by flow cytometry (Beckman CytoFlex, USA). mCherry-expressing EcN coated with calcofluor-white stained YMs were imaged by a confocal laser scanning microscope (TCS-SP8 SR, Leica, Japan).

Cell viability assay

Cell viability was examined with CCK-8 assay. Both EcN and EcN@YM were diluted to an OD_{600} (optical density at 600 nm) value of ~0.15 in LB. Each culture medium (180 μl) was inoculated into a 96-well plate and cultured with 10 μl of CCK-8 solution at 37°C without shaking. The OD_{450} value of the culture was recorded at 1-hour intervals with a Multidetection Microplate reader (BioTek, USA). To evaluate the cell viability of Caco-2 against EcN, YMs, and EcN@YM, Caco-2 cells were seeded in 96-well plates at a density of 8000 cells per well for 24 hours. Then, the cells were treated with 0.1 or 1 mg of YMs and 1×10^7 or 1×10^8 CFUs of the bacteria, respectively. After 24-hour incubation, 10 μl of CCK8 solution was added to each well, and the samples were incubated for 30 min. Cell viability (%) = (sample-blank)/(control-blank) × 100%.

Stability of EcN@YM in simulated gastrointestinal fluids

SGF was prepared by dissolving NaCl (32.0 g) and pepsin (2 g) in 1 liter of deionized water, and the pH was adjusted to 2.0 with a dilute HCl solution. SIF was prepared by dissolving KH_2PO_4 (6.8 g) in 250 ml of deionized water, followed by the addition of 77 ml of 0.2 M NaOH, 200 ml of deionized water, and trypsin (10 g). The pH of the mixture was adjusted to 6.8 with dilute NaOH. SGF, SIF, and cholic acid (0.3 mg/ml) were filtered through a 0.22-μm membrane before use. Equal amounts of EcN and EcN@YM were added into 1 ml of medium including SGF, SIF, and cholic acid, respectively. The samples were cultured at 37°C with shaking at 200 rpm. At predetermined time points, bacteria were centrifuged at 7000 rpm for 10 min and resuspended in 100 μl of PBS. Bacterial counts were determined by culturing the sample in suitable dilution on LB agar plates at 37°C for 24 hours.

Stability of YMs

To measure the stability of YMs, EcN@YM (1×10^8 CFUs) in SIF were cultured at 37°C with shaking at 200 rpm. At the predetermined time points, bacteria were centrifuged at 7000 rpm for 10 min and resuspended in 500 μl of PBS. Then, the samples were measured by LSCM and TEM, respectively. To facilitate LSCM observation, YMs were stained with calcofluor-white.

Stability of β-glucan expression on YMs and EcN@YM

The level of β-glucan was measured by the kit that was used for specific measurement of β-glucan on the yeast cell wall. The same amount of pure YMs and YMs coated on EcN was incubated in SGF and SIF, respectively. Afterward, the samples were centrifuged at 3000 rpm for 15 min and resuspended in 400 μl of 2 M KOH. The samples were incubated on ice for 30 min. Then, 1.6 ml of 1.2 M sodium acetate buffer (pH 3.8) and 40 μl of Glucazyme were added. The mixture was further incubated on ice for 2 min. Then, the samples were incubated at 40°C overnight. Deionized water (10 ml) was added into each tube, and the samples were centrifuged at 3000 rpm for 10 min. Supernate (100 μl) was added into 4 ml of Glucose Determination Reagent (GAPOD Reagent). After a 20-min incubation at 40°C, the

OD value at 510 nm was read with a Multidetection Microplate Reader (BioTek, USA).

Bacterial translocation by M cells in vitro

Caco-2 cells were cultivated at 37°C under 5% CO_2 condition in MEM supplemented with 20% (v/v) fetal bovine serum and 1% (v/v) antibiotic/antimycotic solution. Raji cells were grown in RPMI 1640 medium supplemented with 20% (v/v) fetal bovine serum and 1% (v/v) antibiotic/antimycotic solution. MEM (0.1 and 1.5 ml) supplemented with 10% (v/v) fetal bovine serum was added to the apical and basolateral sides of the Transwell inserts, respectively. Then, the Transwell inserts were preincubated for 30 min in a CO_2 incubator. Afterward, Caco-2 cells (5×10^5) were seeded in the apical side of Transwell inserts (Corning; 1.12 cm^2; pore size, 3 μm) and cultured for 14 days, with the medium replaced every 2 days. After incubation for 14 days, Raji cells (5×10^5) in RPMI 1640/Dulbecco's modified Eagle's medium (1:2) mixture were added to the basolateral chamber of the Transwell plates and cultured for another 7 days. After a quality control check of the cultures by AP activity detection, the culture medium in the basolateral chamber was replaced with a culture medium without antibiotics. The same amount of PBS, EcN, and EcN@YM was added into the apical side of Transwell inserts, respectively. The Transwell plates were incubated at 37°C, and the culture medium at the basolateral chamber was collected at 3-hour intervals. The number of translocated bacteria was determined by plating serial dilutions of the medium on LB agar plates. After 24 hours of culture, the number of bacteria was counted.

Animals

Male Balb/c mice aged 6 to 8 weeks were purchased from Jiesijie Laboratory Animal Technology. The animal research was approved by the Institutional Animal Care and Use Committee of the Shanghai Jiao Tong University School of Medicine and followed the guidelines of the Shanghai Medical Experimental Animal Care.

In vivo survival after oral ingestion

Balb/c mice at 6 to 8 weeks were fed 1×10^8 CFUs of EcN or EcN@YM by oral gavage. At 1, 2, 3, and 4 hours after administration, the mice were imaged by IVIS and then euthanized. The gastrointestinal tracts were harvested and observed by IVIS. To evaluate the survival of the bacteria, tissues including the stomach, small intestine, colon, and cecum as well as their inside contents were separately collected. The samples were grounded and diluted with 1 ml of PBS. The suspensions (100 μl) were withdrawn and spread on solid LB plates. The bacteria were incubated overnight at 37°C before counting.

In vivo uptake of probiotics by M cells

After anesthetizing the mice (Balb/c in 6 to 8 weeks) with enflurane inhalation, PBS, EcN (1×10^8 CFUs), and EcN@YM (1×10^8 CFUs) in 50 μl were injected into the gut loop containing PPs, respectively. After 1.5 hours, the mice were euthanized, and PPs were collected. Partial PPs were collected for bacterial culture, while the remaining portion was fixed with 4% paraformaldehyde and embedded with 30% glycerol. The probiotics in PPs were observed using a Leica RM 2235 microtome (Leica, Microsystems, Wetzlar, Germany). For in vivo probiotic uptake assays, mice were gavaged with 0.2 ml of PBS, EcN (5×10^7 CFUs), and EcN@YM (5×10^7 CFUs), respectively. After 1, 2, 3, and 4 hours, the mice were euthanized, and both the gastrointestinal and MLNs were disengaged from the abdominal cavity for in vivo imaging. Afterward, PPs and MLNs were excised from the intestine for bacterial counting.

Salmonella infection

Salmonella was grown for 8 hours in LB supplemented with kanamycin. After adaption raise for 7 days, mice were daily gavaged with 0.2 ml of PBS and 5×10^7 CFUs of EcN or EcN@YM for 7 days. An amount of 20 mg of streptomycin was administrated after withdrawing the mice from water and food for 4 hours. Mice were orally inoculated with 5×10^7 CFUs of *Salmonella* in PBS 24 hours after streptomycin treatment. Three days after infection, mice were euthanized, and samples were collected for further analysis.

IM operation

After adaption raise for 7 days, mice were daily dosed with 0.2 ml of PBS and 5×10^7 CFUs of EcN or EcN@YM for 7 days and then anesthetized with enflurane inhalation. The abdomen was shaved and sterilized with 75% ethanol. A midline abdominal incision of approximately 1 cm was made, and the small intestine from the ligament of Treitz to the terminal ileum was carefully externalized onto wet gauze using two saline-moistened cotton swabs. Then, the small intestine was systematically touched with two saline-moistened cotton swabs for 5 min for six cycles. Samples were collected 24 hours after IM.

Analysis of cytokines and sIgA

Blood was withdrawn through the eye socket and stored in the tube with heparin. The plasma for the detection of cytokines was isolated by centrifugation with 5000 rpm at 4°C for 10 min. Small intestinal species were cut and scissored longitudinally. Then, the mucus was scrapped out and flushed with 2 ml of cold PBS. The intestinal fluid for the detection of sIgA was harvested by centrifugation with 5000 rpm at 4°C for 10 min. The concentrations of IL-6, TNF-α, and sIgA were detected by enzyme-linked immunosorbent assay kits.

Isolation of lymphocytes and flow cytometric analysis

The PPs and MLNs from the intestine were collected, grounded, and rinsed through 70-μm mesh cell strainers in the six-well plates with RPMI 1640 for harvesting cell suspension. The cell suspension was centrifuged with 3000 rpm for 5 min at 4°C and resuspended with 500 μl of PBS. Concentrations (approximately 1×10^5 cells/ml) were stained with antibodies against surface markers of T cells (CD3e-PerCP Cy5.5, CD4-FITC, and CD8-APC), B cells (CD45R/B220-PE-Cy7, CD138-APC, and IgA-PE), and DCs (CD11c-FITC, CD80-PE, and CD86-APC), respectively. The cells were incubated for 45 min at room temperature. After rinsing with PBS two times, the cells were resuspended in 300 μl of PBS and measured with BD LSRFortessa (BD Bioscience, NY, USA).

Intestinal permeability

After 24 hours of fasting, mice were gavaged with FITC-dextran (4 kDa) at a dose of 400 mg/kg body weight. Blood samples were collected 4 hours after administration, and the fluorescence intensity of the FITC-dextran in plasma was determined using a microplate fluorometer (Infinite M200 PRO, Tecan) with an excitation wavelength of 490 nm and an emission wavelength of 530 nm.

16S sequencing and analysis

The *16S* gene sequencing and analysis were conducted at Biomarker Technologies. The total DNA was extracted from colonic content

and sequenced by building a sequencing library on Illumina HiSeq 2500. The results were stored in FASTQ (referred to as fq) format file, and data analysis was performed on BMKCloud. Alpha diversity that reflects the species richness of individual samples was conducted with ACE index. Beta diversity was analyzed with principal coordinates analysis (PCoA) and nonmetric multidimensional scaling (NMDS).

Statistical analysis

The results are expressed as means ± SD. Statistical analysis was performed using IBM SPSS Statistics 19. The results were analyzed with one-way analysis of variance (ANOVA) with the least significance difference test among three groups. The differences between the two groups were analyzed with Student's *t* tests, giving *P* values of $*P < 0.05$ and $**P < 0.01$.

SUPPLEMENTARY MATERIALS

Supplementary material for this article is available at http://advances.sciencemag.org/cgi/content/full/7/20/eabf0677/DC1

View/request a protocol for this paper from *Bio-protocol*.

REFERENCES AND NOTES

1. C. L. Gentile, T. L. Weir, The gut microbiota at the intersection of diet and human health. *Science* **362**, 776–780 (2018).
2. E. Rinninella, P. Raoul, M. Cintoni, F. Franceschi, G. A. D. Miggiano, A. Gasbarrini, M. C. Mele, What is the healthy gut microbiota composition? A changing ecosystem across age, environment, diet, and diseases. *Microorganisms* **7**, 14 (2019).
3. Y. Gu, X. Wang, J. Li, Y. Zhang, H. Zhong, R. Liu, D. Zhang, Q. Feng, X. Xie, J. Hong, H. Ren, W. Liu, J. Ma, Q. Su, H. Zhang, J. Yang, X. Wang, X. Zhao, W. Gu, Y. Bi, Y. Peng, X. Xu, H. Xia, F. Li, X. Xu, H. Yang, G. Xu, L. Madsen, K. Kristiansen, G. Ning, W. Wang, Analyses of gut microbiota and plasma bile acids enable stratification of patients for antidiabetic treatment. *Nat. Commun.* **8**, 1785 (2017).
4. S. Roy, G. Trinchieri, Microbiota: A key orchestrator of cancer therapy. *Nat. Rev. Cancer* **17**, 271–285 (2017).
5. S. Fujisaka, S. Ussar, C. Clish, S. Devkota, J. M. Dreyfuss, M. Sakaguchi, M. Soto, M. Konishi, S. Softic, E. Altindis, N. Li, G. Gerber, L. Bry, C. R. Kahn, Antibiotic effects on gut microbiota and metabolism are host dependent. *J. Clin. Invest.* **126**, 4430–4443 (2016).
6. L. G. Albenberg, G. D. Wu, Diet and the intestinal microbiome: Associations, functions, and implications for health and disease. *Gastroenterology* **146**, 1564–1572 (2014).
7. X. Li, M. A. Atkinson, The role for gut permeability in the pathogenesis of type 1 diabetes-–A solid or leaky concept? *Pediatr. Diabetes* **16**, 485–492 (2015).
8. F. Imhann, A. Vich Vila, M. J. Bonder, J. Fu, D. Gevers, M. C. Visschedijk, L. M. Spekhorst, R. Alberts, L. Franke, H. M. van Dullemen, R. W. F. Ter Steege, C. Huttenhower, G. Dijkstra, R. J. Xavier, E. A. M. Festen, C. Wijmenga, A. Zhernakova, R. K. Weersma, Interplay of host genetics and gut microbiota underlying the onset and clinical presentation of inflammatory bowel disease. *Gut* **67**, 108–119 (2018).
9. H. Tilg, T. E. Adolph, R. R. Gerner, A. R. Moschen, The intestinal microbiota in colorectal cancer. *Cancer Cell* **33**, 954–964 (2018).
10. L. Muñoz, M. J. Borrero, M. Úbeda, E. Conde, R. Del Campo, M. Rodríguez-Serrano, M. Lario, A. M. Sánchez-Díaz, O. Pastor, D. Díaz, L. García-Bermejo, J. Monserrat, M. Álvarez-Mon, A. Albillos, Intestinal immune dysregulation driven by dysbiosis promotes barrier disruption and bacterial translocation in rats with cirrhosis. *Hepatology* **70**, 925–938 (2019).
11. F. R. Ponziani, S. Bhoori, C. Castelli, L. Putignani, L. Rivoltini, F. Del Chierico, M. Sanguinetti, D. Morelli, F. P. Sterbini, V. Petito, S. Reddel, R. Calvani, C. Camisaschi, A. Picca, A. Tuccitto, A. Gasbarrini, M. Pompili, V. Mazzaferro, Hepatocellular carcinoma is associated with gut microbiota profile and inflammation in nonalcoholic fatty liver disease. *Hepatology* **69**, 107–120 (2019).
12. T. Zuo, F. Zhang, G. C. Y. Lui, Y. K. Yeoh, A. Y. L. Li, H. Zhan, Y. Wan, A. Chung, C. P. Cheung, N. Chen, C. K. C. Lai, Z. Chen, E. Y. K. Tso, K. S. C. Fung, V. Chan, L. Ling, G. Joynt, D. S. C. Hui, F. K. L. Chan, P. K. S. Chan, S. C. Ng, Alterations in gut microbiota of patients with COVID-19 during time of hospitalization. *Gastroenterology* **159**, 944–955.e8 (2020).
13. Y. Taur, K. Coyte, J. Schluter, E. Robilotti, C. Figueroa, M. Gjonbalaj, E. R. Littmann, L. Ling, L. Miller, Y. Gyaltshen, E. Fontana, S. Morjaria, B. Gyurkocza, M.-A. Perales, H. Castro-Malaspina, R. Tamari, D. Ponce, G. Koehne, J. Barker, A. Jakubowski, E. Papadopoulos, P. Dahi, C. Sauter, B. Shaffer, J. W. Young, J. Peled, R. C. Meagher, R. R. Jenq, M. R. M. van den Brink, S. A. Giralt, E. G. Pamer, J. B. Xavier, Reconstitution of the gut microbiota of antibiotic-treated patients by autologous fecal microbiota transplant. *Sci. Transl. Med.* **10**, eaap9489 (2018).
14. E. Y. Huang, T. Inoue, V. A. Leone, S. Dalal, K. Touw, Y. Wang, M. W. Musch, B. Theriault, K. Higuchi, S. Donovan, J. Gilbert, E. B. Chang, Using corticosteroids to reshape the gut microbiome: Implications for inflammatory bowel diseases. *Inflamm. Bowel Dis.* **21**, 963–972 (2015).
15. S. A. Buffington, G. V. Di Prisco, T. A. Auchtung, N. J. Ajami, J. F. Petrosino, M. Costa-Mattioli, Microbial reconstitution reverses maternal diet-induced social and synaptic deficits in offspring. *Cell* **165**, 1762–1775 (2016).
16. E. Mariño, J. L. Richards, K. H. McLeod, D. Stanley, Y. A. Yap, J. Knight, C. McKenzie, J. Kranich, A. C. Oliveira, F. J. Rossello, B. Krishnamurthy, C. M. Nefzger, L. Macia, A. Thorburn, A. G. Baxter, G. Morahan, L. H. Wong, J. M. Polo, R. J. Moore, T. J. Lockett, J. M. Clarke, D. L. Topping, L. C. Harrison, C. R. Mackay, Gut microbial metabolites limit the frequency of autoimmune T cells and protect against type 1 diabetes. *Nat. Immunol.* **18**, 552–562 (2017).
17. F. Gao, Y.-W. Lv, J. Long, J.-M. Chen, J.-m. He, X.-Z. Ruan, H.-b. Zhu, Butyrate improves the metabolic disorder and gut microbiome dysbiosis in mice induced by a high-fat diet. *Front. Pharmacol.* **10**, 1040 (2019).
18. M. T. Cantorna, L. Snyder, J. Arora, Vitamin A and vitamin D regulate the microbial complexity, barrier function, and the mucosal immune responses to ensure intestinal homeostasis. *Crit. Rev. Biochem. Mol. Biol.* **54**, 184–192 (2019).
19. S. Vieira-Silva, G. Falony, E. Belda, T. Nielsen, J. Aron-Wisnewsky, R. Chakaroun, S. K. Forslund, K. Assmann, M. Valles-Colomer, T. T. D. Nguyen, S. Proost, E. Prifti, V. Tremaroli, N. Pons, E. L. Chatelier, F. Andreelli, J.-P. Bastard, L. P. Coelho, N. Galleron, T. H. Hansen, J.-S. Hulot, C. Lewinter, H. K. Pedersen, B. Quinquis, C. Rouault, H. Roume, J.-E. Salem, N. B. Søndertoft, S. Touch, M. C. Consortium, M.-E. Dumas, S. D. Ehrlich, P. Galan, J. P. Gøtze, T. Hansen, J. J. Holst, L. Køber, I. Letunic, J. Nielsen, J.-M. Oppert, M. Stumvoll, H. Vestergaard, J.-D. Zucker, P. Bork, O. Pedersen, F. Bäckhed, K. Clément, J. Raes, Statin therapy is associated with lower prevalence of gut microbiota dysbiosis. *Nature* **581**, 310–315 (2020).
20. F. Sommer, J. M. Anderson, R. Bharti, J. Raes, P. Rosenstiel, The resilience of the intestinal microbiota influences health and disease. *Nat. Rev. Microbiol.* **15**, 630–638 (2017).
21. M. E. Sanders, D. J. Merenstein, G. Reid, G. R. Gibson, R. A. Rastall, Probiotics and prebiotics in intestinal health and disease: From biology to the clinic. *Nat. Rev. Gastroenterol. Hepatol.* **16**, 605–616 (2019).
22. E. G. Pamer, Fecal microbiota transplantation: Effectiveness, complexities, and lingering concerns. *Mucosal Immunol.* **7**, 210–214 (2014).
23. J. Suez, N. Zmora, E. Segal, E. Elinav, The pros, cons, and many unknowns of probiotics. *Nat. Med.* **25**, 716–729 (2019).
24. F. E. Juul, K. Garborg, M. Bretthauer, H. Skudal, M. N. Oines, H. Wiig, O. Rose, B. Seip, J. T. Lamont, T. Midtvedt, J. Valeur, M. Kalager, O. Holme, L. Helsingen, M. Loberg, H. O. Adami, Fecal microbiota transplantation for primary *Clostridium difficile* infection. *N. Engl. J. Med.* **378**, 2535–2536 (2018).
25. L. P. Smits, K. E. C. Bouter, W. M. de Vos, T. J. Borody, M. Nieuwdorp, Therapeutic potential of fecal microbiota transplantation. *Gastroenterology* **145**, 946–953 (2013).
26. S. Wang, M. Xu, W. Wang, X. Cao, M. Piao, S. Khan, F. Yan, H. Cao, B. Wang, Systematic review: Adverse events of fecal microbiota transplantation. *PLOS ONE* **11**, e0161174 (2016).
27. M. J. Blaser, Fecal microbiota transplantation for dysbiosis -–- Predictable risks. *N. Engl. J. Med.* **381**, 2064–2066 (2019).
28. M. Levy, A. A. Kolodziejczyk, C. A. Thaiss, E. Elinav, Dysbiosis and the immune system. *Nat. Rev. Immunol.* **17**, 219–232 (2017).
29. D. Zheng, T. Liwinski, E. Elinav, Interaction between microbiota and immunity in health and disease. *Cell Res.* **30**, 492–506 (2020).
30. O. Pabst, E. Slack, IgA and the intestinal microbiota: The importance of being specific. *Mucosal Immunol.* **13**, 12–21 (2020).
31. N. J. Mantis, N. Rol, B. Corthésy, Secretory IgA's complex roles in immunity and mucosal homeostasis in the gut. *Mucosal Immunol.* **4**, 603–611 (2011).
32. X. Zhou, X. Zhang, S. Han, Y. Dou, M. Liu, L. Zhang, J. Guo, Q. Shi, G. Gong, R. Wang, J. Hu, X. Li, J. Zhang, Yeast microcapsule-mediated targeted delivery of diverse nanoparticles for imaging and therapy via the oral route. *Nano Lett.* **17**, 1056–1064 (2017).
33. M. Aouadi, G. J. Tesz, S. M. Nicoloro, M. Wang, M. Chouinard, E. Soto, G. R. Ostroff, M. P. Czech, Orally delivered siRNA targeting macrophage Map4k4 suppresses systemic inflammation. *Nature* **458**, 1180–1184 (2009).
34. P. Feng, Z. Cao, X. Wang, J. Li, J. Liu, On-demand bacterial reactivation by restraining within a triggerable nanocoating. *Adv. Mater.* **32**, 2002406 (2020).
35. Z. Cao, X. Wang, Y. Pang, S. Cheng, J. Liu, Biointerfacial self-assembly generates lipid membrane coated bacteria for enhanced oral delivery and treatment. *Nat. Commun.* **10**, 5783 (2019).

36. N. Lahav-Mankovski, P. K. Prasad, N. Oppenheimer-Low, G. Raviv, T. Dadosh, T. Unger, T. M. Salame, L. Motiei, D. Margulies, Decorating bacteria with self-assembled synthetic receptors. *Nat. Commun.* **11**, 1299 (2020).
37. Z. Cao, S. Cheng, X. Wang, Y. Pang, J. Liu, Camouflaging bacteria by wrapping with cell membranes. *Nat. Commun.* **10**, 3452 (2019).
38. X. Wang, Z. Cao, M. Zhang, L. Meng, Z. Ming, J. Liu, Bioinspired oral delivery of gut microbiota by self-coating with biofilms. *Sci. Adv.* **6**, eabb1952 (2020).
39. M. Banar, M. Emaneini, R. Beigverdi, R. Fanaei Pirlar, N. Node Farahani, W. B. van Leeuwen, F. Jabalameli, The efficacy of lyticase and β-glucosidase enzymes on biofilm degradation of *Pseudomonas aeruginosa* strains with different gene profiles. *BMC Microbiol.* **19**, 291 (2019).
40. S. E. Howe, D. J. Lickteig, K. N. Plunkett, J. S. Ryerse, V. Konjufca, The uptake of soluble and particulate antigens by epithelial cells in the mouse small intestine. *PLOS ONE* **9**, e86656 (2014).
41. A. Beloqui, D. J. Brayden, P. Artursson, V. Préat, A. des Rieux, A human intestinal M-cell-like model for investigating particle, antigen and microorganism translocation. *Nat. Protoc.* **12**, 1387–1399 (2017).
42. S. Fukuda, K. Hase, H. Ohno, Application of a mouse ligated Peyer's patch intestinal loop assay to evaluate bacterial uptake by M cells. *J. Vis. Exp.* , e3225 (2011).
43. M. Martínez-López, S. Iborra, R. Conde-Garrosa, A. Mastrangelo, C. Danne, E. R. Mann, D. M. Reid, V. Gaboriau-Routhiau, M. Chaparro, M. P. Lorenzo, L. Minnerup, P. Saz-Leal, E. Slack, B. Kemp, J. P. Gisbert, A. Dzionek, M. J. Robinson, F. J. Rupérez, N. Cerf-Bensussan, G. D. Brown, D. Bernardo, S. L. Gut-Landmann, D. Sancho, Microbiota sensing by mincle-syk axis in dendritic cells regulates interleukin-17 and -22 production and promotes intestinal barrier integrity. *Immunity* **50**, 446–461.e9 (2019).
44. D. Rios, M. B. Wood, J. Li, B. Chassaing, A. T. Gewirtz, I. R. Williams, Antigen sampling by intestinal M cells is the principal pathway initiating mucosal IgA production to commensal enteric bacteria. *Mucosal Immunol.* **9**, 907–916 (2016).
45. B. Corthésy, Multi-faceted functions of secretory IgA at mucosal surfaces. *Front. Immunol.* **4**, 185 (2013).
46. J. J. Cebra, S. B. Periwal, G. Lee, F. Lee, K. E. Shroff, Development and maintenance of the gut-associated lymphoid tissue (GALT): The roles of enteric bacteria and viruses. *Dev. Immunol.* **6**, 13–18 (1998).
47. L. Xiao, C. Gong, Y. Ding, G. Ding, X. Xu, C. Deng, X. Ze, P. Malard, X. Ben, Probiotics maintain intestinal secretory immunoglobulin A levels in healthy formula-fed infants: A randomised, double-blind, placebo-controlled study. *Benef. Microbes* **10**, 729–739 (2019).
48. J. J. Bunker, A. Bendelac, IgA responses to microbiota. *Immunity* **49**, 211–224 (2018).
49. E. Soares, R. Cordeiro, H. Faneca, O. Borges, Polymeric nanoengineered HBsAg DNA vaccine designed in combination with β-glucan. *Int. J. Biol. Macromol.* **122**, 930–939 (2019).
50. D. An, Y. Apidianakis, A. L. Boechat, R. L. Baldini, B. C. Goumnerov, L. G. Rahme, The pathogenic properties of a novel and conserved gene product, KerV, in proteobacteria. *PLOS ONE* **4**, e7167 (2009).
51. J. Xu, M. A. Mahowald, R. E. Ley, C. A. Lozupone, M. Hamady, E. C. Martens, B. Henrissat, P. M. Coutinho, P. Minx, P. Latreille, H. Cordum, A. Van Brunt, K. Kim, R. S. Fulton, L. A. Fulton, S. W. Clifton, R. K. Wilson, R. D. Knight, J. I. Gordon, Evolution of symbiotic bacteria in the distal human intestine. *PLOS Biol.* **5**, e156 (2007).
52. S.-S. Lin, R.-Q. Zhang, L. Shen, X.-J. Xu, K. Li, A.-V. Bazhin, J. Fichna, Y.-Y. Li, Alterations in the gut barrier and involvement of Toll-like receptor 4 in murine postoperative ileus. *Neurogastroenterol. Motil.* **30**, e13286 (2018).
53. A. P. Corfield, The interaction of the gut microbiota with the mucus barrier in health and disease in human. *Microorganisms* **6**, 78 (2018).
54. S. F. Assimakopoulos, C. Triantos, I. Maroulis, C. Gogos, The role of the gut barrier function in health and disease. *Gastroenterology Res.* **11**, 261–263 (2018).
55. M. A. Odenwald, J. R. Turner, The intestinal epithelial barrier: A therapeutic target? *Nat. Rev. Gastroenterol. Hepatol.* **14**, 9–21 (2017).
56. V. A. Pedicord, A. A. K. Lockhart, K. J. Rangan, J. W. Craig, J. Loschko, A. Rogoz, H. C. Hang, D. Mucida, Exploiting a host-commensal interaction to promote intestinal barrier function and enteric pathogen tolerance. *Sci. Immunol.* **1**, eaai7732 (2016).

Acknowledgments

Funding: This work was financially supported by the National Natural Science Foundation of China (21875135), the Recruitment Program of Global Youth Experts of China (D1410022), the Shanghai Municipal Education Commission–Gaofeng Clinical Medicine Grant Support (20181704), and the Innovative Research Team of High-Level Local Universities in Shanghai (SSMU-ZLCX20180701). **Author contributions:** J.Liu conceived and designed the experiments. S.L., S.M., J.Li, W.H., and C.P. performed all experiments. All authors analyzed and discussed the data. S.L. and J.L. wrote the paper. **Competing interests:** The authors declare that they have no competing interests. **Data and materials availability:** All data needed to evaluate the conclusions in the paper are present in the paper and/or the Supplementary Materials. Additional data related to this paper may be requested from the authors.

Submitted 1 October 2020
Accepted 23 March 2021
Published 12 May 2021
10.1126/sciadv.abf0677

Citation: S. Lin, S. Mukherjee, J. Li, W. Hou, C. Pan, J. Liu, Mucosal immunity–mediated modulation of the gut microbiome by oral delivery of probiotics into Peyer's patches. *Sci. Adv.* **7**, eabf0677 (2021).